MALAYSIAN JOURNAL OF SCIENCE
MJS
ISSN 1394-3065

Regular Issue

Malaysian Journal of Science 43(1): 22-33 (Mar 2024) https://mjs.um.edu.my

# BACTERIAL CELLULOSE INCORPORATED ZINC PHOSPHATE NANOCOMPOSITE FOR ANTIBACTERIAL AGENT AND AIR PARTICULATE MATTER FILTRATION

Nurhidayah Nurhidayah[1a], La Ode Ahmad Nur Ramadhan[2b]*, Abdul Haris Watoni[3b], Laode Abdul Kadir[4b], Muhammad Daffa Rahmatullah[5b], and Cindy Agriningsih Haruna[6b]

**Abstract:** This study investigates the synthesis and the antibacterial properties of bacterial cellulose (BC) incorporated zinc phosphate nanocomposite-mediated dragon fruit extract (BC-ZP-DF). The composite was prepared by a three-step process that involved bacterial cellulose (BC), zinc phosphate (ZP), and nanocomposite BC-ZP synthesis. BC was prepared by fermenting coconut water with the components of ammonium sulfate, acetic acid, and *Acetobacter xylinum* culture. Zinc phosphate was made through the green synthesis method by reacting zinc nitrate and diammonium hydrogen phosphate using a sensitizer agent from red dragon fruit peel extract (DF) with volume variations of 5, 10, 20, 30, 40, and 50 mL. The composite was prepared by immersing BC with zinc phosphate. Phase crystallinity, functional group, and morphology of the samples were characterized using XRD, FTIR, and SEM. It was found that the nanocomposite was constructed by the nano green of zinc phosphate in the form of a hopeite structure with antibacterial $PO_4^{3-}$ and OH functional groups. Morphological analysis using SEM revealed that the nanocomposites contained various small powder grains. Based on the FTIR spectrum, XRD pattern, and surface morphology of composite film, the incorporation of zinc phosphate in the BC framework was confirmed. The antibacterial activity tests of nanocomposite films using *Staphylococcus aureus* and *Pseudomonas aeruginosa* bacteria revealed that the nanocomposite was highly effective in inhibiting both bacteria, and the nanocomposite BC-ZP-DF10 film had the strongest inhibition. The results of the air filter test exhibited that the composition was efficient on all films with the highest percent of efficiency (%E) of 90.10%.

***Keywords:*** *Zinc phosphate, bacterial cellulose, antibacterial, particulate matter filtration, filtration*

## 1. Introduction

In recent years, rapid industrial growth has led to a rise in air pollution worldwide (Lippi et al., 2022). Air pollution containing particulate matter (PM) is an increasingly prevalent environmental issue that threatens human health, ecosystems, and the climate. The lethal effects of particulate pollutants vary mainly by their diameter. Typically, PM larger than 10 µm in diameter cannot penetrate the human lung and will instead be efficiently filtered and captured by the respiratory organs. Smaller PM with a diameter of 2.5 to 10 µm and less than 2.5 µm are called PM10 and PM2.5, respectively. These are harmful to humans because they can easily and unabatedly penetrate the lungs (Wu et al., 2022). Recent reports indicate that prolonged exposure to environmental particulates can elicit respiratory and cardiovascular illnesses, such as stroke, atherosclerosis, bronchitis, and asthma (Xing et al., 2016). In addition, atmospheric chemicals, bacteria, microorganisms, and viruses use PM as a carrier substance to penetrate the human body, resulting in the spread of various diseases among humans (Wu et al., 2022; Xing et al., 2016). Therefore, solutions to prevent the harmful effects of air particulates are urgently needed. One such solution is air quality control, both indoors and in car spaces so that particulates, dust, and bioaerosols containing harmful microorganisms can be filtered out of the air inhaled by humans. To overcome the problem of air pollution, researchers have developed functional advanced materials, such as the High-Efficiency Particulate Air (HEPA) Filter technology. Currently, HEPA technology, one component of which is a filter matrix, is effectively capable of filtering 99.97% of very fine particles up to 0.3 µm (Franchitti et al., 2020). This technology has been utilized for cleaning static air environments in various fields, such as isolation rooms in hospitals, biotechnology laboratory rooms, and portable air purifiers (Franchitti et al., 2020). However, the existing filter matrix material is not environmentally friendly because it is dominantly made of synthetic polymer raw materials. Therefore, alternative raw materials that are environmentally friendly and sustainable need to be identified. One potential option for using natural polymers as composite material is cellulose.

BC is a naturally biodegradable cellulose with fiber diameters ranging from 20 to 100 nm (Jonsirivilai et al., 2022). Due to its hydrophilic characteristics, BC has a high water-holding capacity. It also has high mechanical strength with a smaller fiber diameter measuring 3–4 nm thick, and it is relatively more affordable to produce. The fiber is biocompatible, non-toxic, and precisely

**Authors information:**
[a]Department of Chemistry, Postgraduate, Halu Oleo University, Kendari, INDONESIA. E-mail: nhayahidayah@gmail.com[1]
[b]Department of Chemistry, Faculty of Mathematics and Natural Science, Halu Oleo University, Kendari, INDONESIA. E-mail: laode.ramadhan@uho.ac.id[2]; ahwatoni@uho.ac.id[3]; laode.kadir90@uho.ac.id[4]; mdaffa2709@gmail.com[5]; cindyaharuna@gmail.com[6]
*Corresponding Author: laode.ramadhan@uho.ac.id

Received: December 9, 2022
Accepted: May 7, 2023
Published: March 31, 2024



DOI:https//doi.org/10.22452/mjs.vol43no1.3
Malaysian Journal of Science 43(1): 22-33 (March 2024)

structured with a large surface area (Manoukian et al., 2019). Due to its high surface area, nanofiber diameter, and high hydrophilicity, the use of BC as an air filter membrane produces a more potent and efficient filtration effect than commercial membranes (Manoukian et al., 2019). The production of air filters takes into consideration numerous characteristics. Good quality filters are characterized by a low-pressure drop, which is reflected through high permeability and a wide surface area that will support the absorption of more particles. Nowadays, BC is one of the most commonly used materials for air filtration, as it can capture aerosol particles from gas streams by their fibers via Brownian diffusion, direct interception, inertial impact, gravity regulation, and electrostatic deposition. The airflow velocity, particle characteristics, and shape of the air filtering material all directly influence this mechanism, which regulates the air filtration process (Lippi et al., 2022). The BC used in this research is Nata de Coco cellulose. Nata de Coco cellulose is a cellulose polymer sourced from abundant coconut water fermentation using the *Acetobacter xylinum* bacteria (Mulyasuryani & Mustaghfiroh, 2019). Furthermore, BC has unique physical and mechanical characteristics, such as high porosity, high crystallinity, exceptional mechanical strength, and a significant water-holding capacity (Nugroho & Aji, 2015). BC composited with zinc phosphate nanoparticles can potentially be used as an excellent antimicrobial matrix for high-efficiency particulate absorbing (HEPA) filters. Nanoparticles are well known for their excellent antimicrobial properties (Sabherwal et al., 2017). An essential, multipurpose inorganic substance known as zinc phosphate is also a type of often utilized luminous host material (Kimbonguila et al., 2019). Zinc phosphate can be synthesized from zinc nitrate and different phosphate compounds, including phosphoric acid (Kopel et al., 2018), sodium dihydrogen phosphate (Wang et al., 2011), disodium hydrogen phosphate (Horky et al., 2019), sodium pyrophosphate (Kopel et al., 2018; Onoda & Haruki, 2016), trisodium phosphate (Wang et al., 2011), or sodium triphosphate (Grzmil et al., 2007; Onoda & Haruki, 2016). However, zinc phosphate produced from these precursors exhibits a fairly low photocatalytic action (Grzmil et al., 2007; Kopel et al., 2018). Therefore, it is necessary to find alternative precursors to produce zinc phosphate that has a high photocatalytic action. One such precursor is diammonium hydrogen phosphate.

Zinc phosphate can be reacted with plant extracts containing dyes as sensitizing agents. In addition to reducing the particle size, this reaction is expected to increase antibacterial activity. The antimicrobial properties of nanoparticles are due to their ability to deface bacterial cell walls, disrupt cell metabolism, and inhibit microbial cell formation (Sabherwal et al., 2017). Synthesis of zinc phosphate nanoparticles was performed through an environmentally friendly green synthesis approach with a sensitizing agent from the waste extract of the red dragon fruit. Red dragon fruit peel extract has potential use as a sensitizing agent because it contains several active compounds including flavonoids, alkaloids, and terpenoids (Rahmayanti et al., 2019). Thus far, there has been no research exploring the use of red dragon fruit peel extract and diammonium hydrogen phosphate in the synthesis of zinc phosphate and its use in antibacterial composites on HEPA filter membranes. Hence, this research was conducted to evaluate the zinc phosphate nanoparticle material and its antibacterial characteristics under preparation with the addition of extract-sensitizing agents of the red dragon fruit peel plant. The findings of the study were assessed based on visual observation and characteristic determination of the material using UV-Vis (Ultraviolet-Visible) spectrophotometer, FTIR (Fourier Transform Infrared) spectrophotometer, XRD (X-ray diffraction), and SEM (Scanning Electron Microscope). The composite was then tested for its antibacterial activity and its efficiency as an air filter. The synthesized composite film has a greater advantage as an air particulate matter filter due to the presence of zinc phosphate and red dragon fruit peel extract, both of which have the good antibacterial activity. In comparison, previous studies conducted by Liu et al. (2017) only explored its use as particulate matter filters.

## 2. Materials and Methods

**Materials**

In this study, the materials used were dragon fruit peel, coconut water, aquades, ethanol p.a (Emsure Merck), sugar ($C_6H_{12}O_6$), ammonium sulfate (ZA), glacial acetic acid p.a (Emsure Merck), *Acetobacter xylinum* stater, nutrient agar (Emsure Merck), nutrient broth (Emsure Merck), *P. aeruginosa*, *S. aureus*, Whatman filter paper No. 40, $Zn(NO_3)_2.6H_2O$ p.a (Emsure Merck), $(NH_4)_2HPO_4$ p.a (Emsure Merck), NaOH p.a (Emsure Merck), and NaCl p.a (Emsure Merck).

The instruments used were XRD (Phillips), FTIR Spectrophotometer (Shimadzu), UV-Vis Spectrophotometer (Vernier), Scanning Electron Microscope (JEOL JSM-6360), PM Analyzer (Kailishen SYSC-BR8), Digital Optic Microscope (OEM), Rotary Evaporator (Buchi), Dessicator (Duran), oven (YNC-OV50L), Hydraulic Hot Press Machine (HTM 634), and Mini Aerosol Generator (Tasco).

**Methods**

**Preparation of Red Dragon Fruit Peel Extract and Bacterial Cellulose**

To extract the dragon fruit peel waste, we used a maceration method adapted from Manihuruk et al. (2017). First, 500 g of simplicia powder was added to a 1000 ml-Beaker glass, and 96% ethanol was added. Then, it was macerated for 3×24 hours by the filtering procedure every 24 hours, and the simplicia was soaked again with a new solvent. The filtration results were then evaporated for three hours using a rotary evaporator at 45 °C to obtain the red dragon fruit extract.

Next, BC preparation was adapted from Nugroho and Aji (2015) by fermenting coconut water with the ingredients of ammonium sulfate, acetic acid, and *Acetobacter xylinum* culture. This was done at 28 °C for 10 days until the BC sheet was obtained. This sheet was used as a matrix in the synthesis of filter composites.


DOI:https//doi.org/10.22452/mjs.vol43no1.3
Malaysian Journal of Science 43(1): 22-33 (March 2024)

**Synthesis of Zinc Phosphate-Red Dragon Fruit Peel Extract**

The synthesis method was adapted from Pavel et al. (2019). First, 4.46 g of $Zn(NO_3)_2.6H_2O$ was dissolved in distilled water and heated to 60 °C, followed by the addition of 1.32 g of $(NH_4)_2HPO_4$ in 20 ml of distilled water, and incorporation of the red dragon fruit extract solution. The mixture was stirred until a precipitate was formed. The suspension produced was stirred for two hours and cooled, and water was added to reach 100 ml. The suspension was then centrifuged and decanted (Horky et al., 2019). The composition ratio of the mixture of materials can be seen in Table 1. The outcome of the synthesis was characterized by observing their functional groups using an FTIR Spectrophotometer, their crystalline and oxide structures using an X-ray diffractometer, their morphology using SEM, and their nanoparticle stability using a UV-Vis Spectrophotometer. Antimicrobial actions were tested using the paper disc method.

**Table 1**. Synthetic composition zinc phosphate

| Sample code* | $Zn(NO_3)_2.6H_2O$ (grams) | $(NH_4)_2HPO4$ (grams) | Extract of dragon fruit peel (ml) |
|---|---|---|---|
| ZP | 4.46 | 1.32 | 0 |
| ZP-DF5 | 4.46 | 1.32 | 5 |
| ZP-DF10 | 4.46 | 1.32 | 10 |
| ZP-DF20 | 4.46 | 1.32 | 20 |
| ZP-DF30 | 4.46 | 1.32 | 30 |
| ZP-DF40 | 4.46 | 1.32 | 40 |
| ZP-DF50 | 4.46 | 1.32 | 50 |

*ZP is zinc phosphate, and ZP-DF5 to ZP-DF50 are zinc phosphate and extract.

**Synthesis of BC-zinc Phosphate Composite Film-Mediated Red Dragon Fruit Peel Extract**

The composite film of BC was neutralized with 1% w/v NaOH and then rinsed with distilled water until the pH was neutral. The composite was then modified into pieces of film sheets sized 4x9 cm. The film was pressed using a hot press to reduce its water content. Subsequently, the film was composited with synthesized nanoparticles (Table 1) by immersing it for 1x24 hours. The film was then pressed again using a hot press and dried in an oven at 150 °C for 10 minutes. The films were removed from the oven and cooled in a desiccator for ± 15 minutes to obtain a composite film with an average thickness of 0.20 mm; they were coded BC-ZP, BC-ZP-DF5, BC-ZP-DF10, BC-ZP-DF15, BC-ZP-DF20, BC-ZP-DF30, BC-ZP-DF40, and BC-ZP-DF50. The composites were then characterized using FTIR, XRD, and SEM.

**Antibacterial Testing**

Antibacterial testing was conducted using the paper disc method. The suspension of the test bacteria (*S. aureus* and *P. aeruginosa*) was poured into an Erlenmeyer containing NA media to be homogenized. The NA medium was poured into each petri dish, then gently shaken to form a figure eight to spread the bacterial culture evenly, and allowed to stand until the media solidified. The filter paper that had been cut into pieces utilizing a hole jab was then dipped into the test sample using sterile tweezers. The mixture was transferred to an NA medium containing *S. aureus* and *P. aeruginosa* bacteria cultures in the aseptically arranged distance, labeled according to the treatment group, and incubated for 24 hours at 37 °C (Massoud & Saffari, 2020). After 24 hours, a clearer area was observed around the sample area. The clearer area indicates the inhibition zone for the growth of *S. aureus* and *P. aeruginosa*. The inhibition zone formed was measured using a caliper. Antibacterial activity was measured or calculated using Equation 1 as follows:

$$Z = \frac{(D1-Dfc) + (D2-Dfc) + (D3-Dfc)}{3} \quad (1)$$

Where: Z = Zone clear (mm), D1= Vertical diameter (mm), D2 = Horizontal diameter (mm), D3 = Diagonal diameter (mm), and Dfc = Film diameter composite (mm). Based on the calculation of the inhibition zone diameter, the antibacterial activity of the composite can be categorized as follows: diameter > 20 mm = very strong, 11-20 mm = strong, 6-10 = moderate, and < 5 = weak (Massoud & Saffari, 2020).

**Air Filter Test**

The performance of the air filter system was analyzed by systems using NaCl aerosol as recommended by Konda et al. (2020). The test was carried out at 1 atm and 29 °C. The filter was tested for its ability to filter NaCl aerosol, where nano-sized particles were generated using a NaCl aerosol generator. The collection of NaCl aerosol particles was then pumped in through the test filter. The test filter used was a circular filter film with a diameter of 2.54 cm. The concentration of particles before they pass through the filter ($C_i$) and after they pass through the filter ($C_f$) was measured using the Particulate Matter (PM) Analyzer (SYSC BR-8). The performance of the air filter media is indicated by the results of the efficiency measurement, as expressed by Equation 2.

$$\%E = \frac{Ci-Cf}{Ci} x100 \quad (2)$$

where % $E$ is the percent of efficiency, $C_f$ and $C_i$ are the number of particles after and before passing through the filter, respectively. The air filter test scheme is depicted in Figure 1.


DOI:https//doi.org/10.22452/mjs.vol43no1.3
Malaysian Journal of Science 43(1): 22-33 (March 2024)

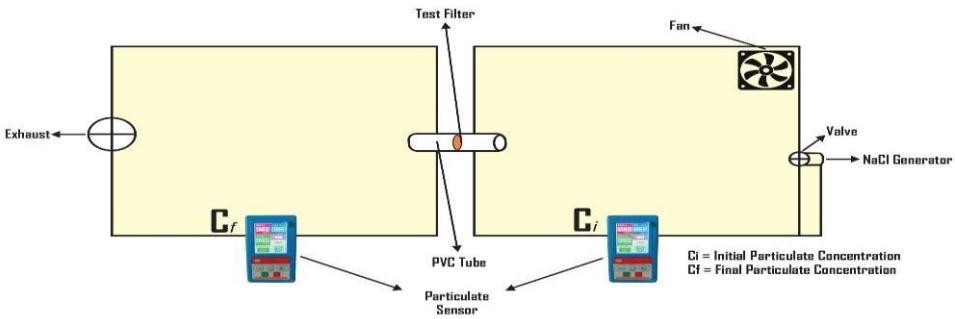


**Figure 1**. The illustration of the air filter test scheme

## 3. Results

**Red Dragon Fruit Peel Extract**

The extraction process of the red dragon fruit peel waste produced a concentrated extract of 160 ml with a yield of red dragon fruit peel extract of 10.6%.

**Synthesis of Zinc Phosphate-Red Dragon Fruit Peel Extract**

The resulting zinc phosphate was in the form of powder with various colors. The synthesized zinc phosphate yield can be seen in Table 2.

**Table 2**. Yield of zinc phosphate-red dragon fruit peel extract

| Sample Code | Yield (%) |
|---|---|
| ZP | 60.46 |
| ZP-DF5 | 63.73 |
| ZP-DF10 | 89.34 |
| ZP-DF20 | 95.73 |
| ZP-DF30 | 111.48 |
| ZP-DF40 | 171.76 |
| ZP-DF50 | 60.46 |

The yield of zinc phosphate increased when more extract was used. This can be observed in the yield obtained from ZP-DF5 to ZP-DF40, which increased periodically to reach a maximum limit at ZP-DF40 and decreased at ZP-DF50. This is because the penetration of the synthesizer agent into the material had decreased, so less zinc phosphate was formed in the material.

Mixing red dragon fruit peel extract with zinc phosphate produced a precipitate that varied from brown to yellowish brown (Figure 2). This color change indicates a reaction in the mixture caused by the sensitizing agent used in this study, the red dragon fruit peel extract. This extract contains dyes, namely anthocyanin compounds. The conjugated double bond with the chromophore moiety in the anthocyanin backbone allows for light energy to be absorbed with maximum absorbance in the visible light range. As the length and number of the double bonds conjugated to anthocyanins increase, the color becomes stronger (Nurtiana, 2019). The dye molecules are stimulated during this sensitization process by absorbing visible light, and electrons are then moved from the highest-occupied molecular orbital (HOMO) to the lowest-vacant molecular orbital (LUMO) (Dil et al., 2019).

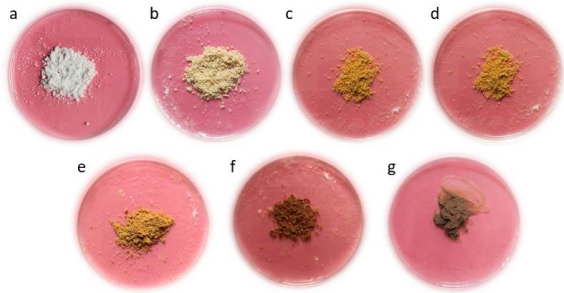


**Figure 2.** Products of the synthesis of zinc phosphate: (a) ZP, (b) ZP-DF5, (c) ZP-DF10, (d) ZP-DF20, (e) ZP-DF30, (f) ZP-DF40 and (g) ZP-DF50.

**Stability Analysis of Zinc Phosphate-Red Dragon Fruit Peel Extract**

The UV-Vis absorbance spectrum of transparent colloidal solution was observed using a UV-Vis spectrophotometer in the wave range of 200-800 nanometers. Measuring the zinc phosphate nanoparticles-red dragon fruit peel extract using a UV-Vis spectrophotometer caused an excitation phenomenon due to the interaction of light with precious metal nanoparticles called the surface plasmon resonance (SPR) phenomenon (Budi, 2017). The SPR phenomenon is related to the color of the zinc phosphate nanoparticle solution (Haiss et al., 2008; Zakir & Budi, 2016).

The SPR absorption band is a collection of electron oscillations (Haiss et al., 2008). The collection of electron oscillations that can be observed from the change of color of the solution from yellow to dark brown shows the distribution of zinc nanoparticles in the solution (Budi, 2017). Based on UV-Vis analysis results, the stability of the complex compound of zinc phosphate nanoparticles from the Red Dragon fruit peel extract was reasonably good. Based on the interaction of the solution with UV-Vis light, the zinc phosphate was stable for 30 minutes as seen from the stability of the curve of zinc phosphate nanoparticles-red dragon fruit peel extract (Figure 3). Due to the visible light being absorbed during this sensitization process, dye molecules from dragon fruit peel extract are stimulated, and electrons are then moved from the highest occupied molecular orbital (HOMO)


DOI:https//doi.org/10.22452/mjs.vol43no1.3
Malaysian Journal of Science 43(1): 22-33 (March 2024)

to the lowest vacant molecular orbital (LUMO). These excited electrons are eventually transferred to the conduction band of the photocatalyst molecule semiconductor, resulting in the formation of highly reactive superoxide anions ($O_2^-$) and/or hydroxyl radicals (•OH) (Ghosh et al., 2020). The maximum wavelength shifts to a lower value as the concentration of $Zn(NO_3)_2$ increases, which means that the interaction energy between organic compounds in the extract and Zn increases.

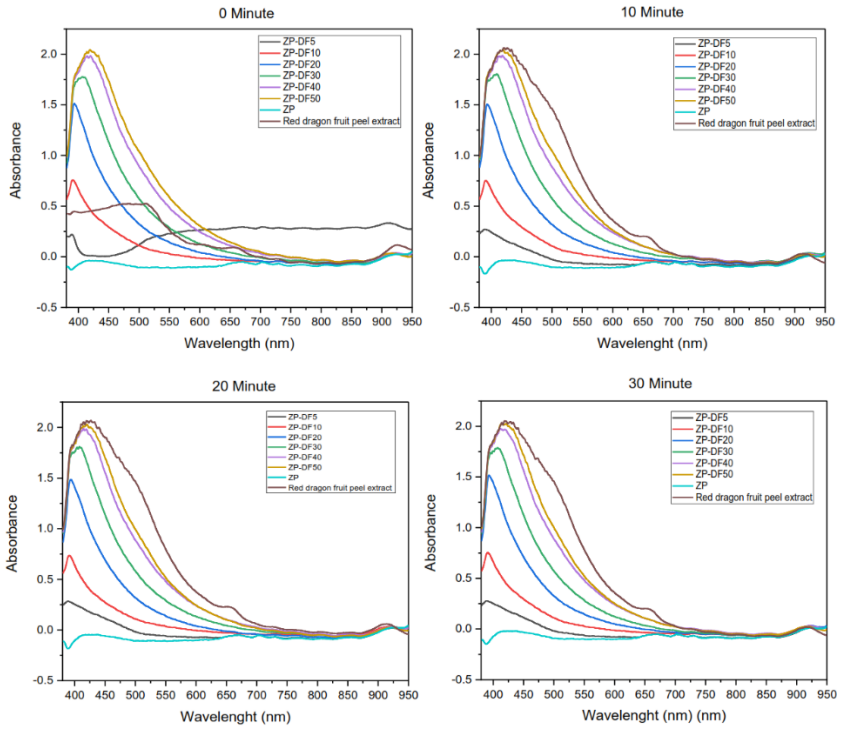


**Figure 3.** UV-Vis absorbance spectrum of zinc phosphate nanoparticles-red dragon fruit peel extract at intervals of (a) 0 minutes, (b) 10 minutes, (c) 20 minutes, and (d) 30 minutes.

**Functional Group Analysis of Zinc Phosphate Nanoparticles-Red Dragon Fruit Peel Extract Using an Ftir Spectrophotometer**

Based on the FTIR data in Figure 4, there is a wide band data centered on 3334–3353 $cm^{-1}$ for all samples (extract, ZP-DF5, ZP-DF10, ZP-DF20, ZP-DF30, ZP-DF40, and ZP-DF50), which identifies the –OH stretching vibration (Ghosh et al., 2020; Zhang et al., 2019). In addition, a strong vibrational band at 1618–1643 $cm^{-1}$ is associated with $H_2O$ bonds. The FTIR spectrum exhibits characteristic bands associated with $PO_4^{3-}$ and $H_2O$. Bandwidths are exhibited at 500 ~ 700 $cm^{-1}$ (peak at 632 $cm^{-1}$) and 900 ~ 1300 $cm^{-1}$ (ref: 900 ~ 1200 $cm^{-1}$) for ZP-DF5, ZP-DF10, ZP-DF20, ZP-DF30, ZP-DF40, and ZP-DF50 nanoparticles, respectively. Each spectrum is associated with the presence of $PO_4^{3-}$ flexible and Zn strain vibration groups. Therefore, this peak is not visible in the extracted spectrum because it does not contain zinc. From the synthesized zinc phosphate, a very strong, recognizable peak at 1010 $cm^{-1}$ was caused by the antisymmetric stretching of $PO_4^{3-}$ (Wang et al., 2011).

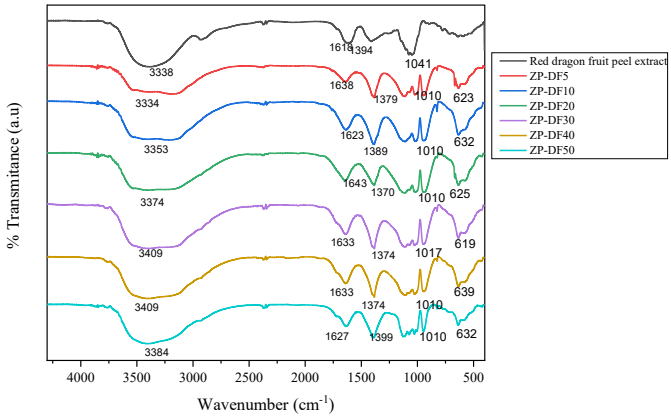


**Figure 4.** FTIR spectrum of zinc phosphate nanoparticles-red dragon fruit peel extract

**Crystallite Size Analysis of Zinc Phosphate Nanoparticles**

The results of zinc phosphate synthesis are supported by an X-ray diffractogram, which is compared to the standard diffraction pattern from the Crystallography Open Database (COD) zinc phosphate with an entry number of 95-900-0523. The existing peak 2θ data are 9,54º, 16,55º, 17,31º, 18,09º, 19,23º, 19,93º, 22,23º, 22,82º, 25,57º, 26,14º, 31,26º, 34,21º, 39,26º, 46,82º, and 49,89º. From the diffractograms of ZP-DF20 to ZP-DF50, some narrow and small intensity peaks of 2θ over the range 16,70º-18,28º are evident. This is thought to be derived from


DOI:https//doi.org/10.22452/mjs.vol43no1.3
Malaysian Journal of Science 43(1): 22-33 (March 2024)

diammonium hydrogen phosphate residues and extracts. However, the overall results of the analysis prove that $Zn_3(PO_4)_2$ has a good match with the Hopeite structure. The XRD pattern of zinc phosphate-red dragon fruit extract powder is shown in Figure 5.

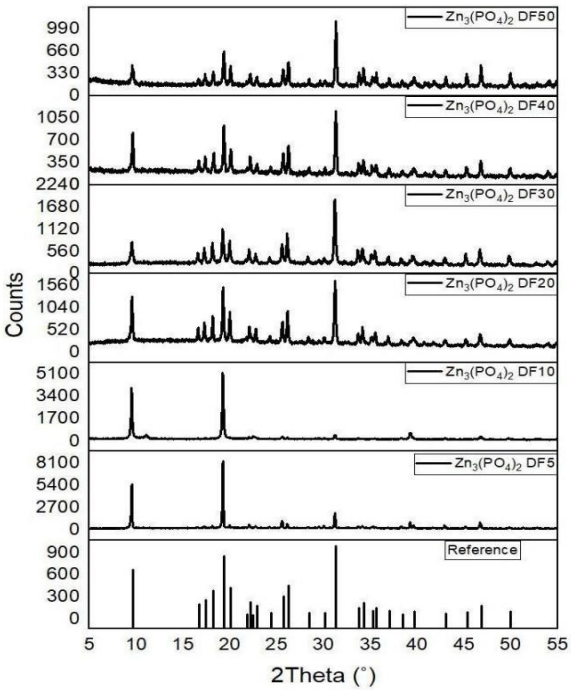


**Figure 5.** XRD spectrum of zinc phosphate nanoparticles-red dragon fruit peel extract

From the XRD characterization data, the size of the crystal could be estimated by using the Scherrer formula

$$D = \frac{\kappa\lambda}{\beta cos(\theta)} \quad (4)$$

where length wave X-rays are used, and = angle diffraction, K = is large constant - depends on factors from the crystal, diffraction (hkl) plane and definition quantity β used, whether - as Full Width at Half Maximum (FWHM) or Integral Breadth of a peak. True K value varied from 0.62 to 2.08. The typical value used for K is 0.94 if β is FWHM and 0.89 for Integral Breadth (Franchitti et al., 2020; Wu et al., 2022). The equation observed that the wide peak varied with angle 2θ in the form of cos (θ). A defined quantity β was FWHM and the constant K was chosen to be 0.94. With the thereby obtained number of N sizes crystals under field, the measured hkl are presented in Table 3. ZP-DF10 shows the average size crystal, the smallest of which is 37.48 nm. The existence of an additional extract peel fruit dragon could influence the size of the resulting crystals. This has been proven with a comparison with pure zinc phosphate, which was researched previously by Grzmil et al. who produced an average crystallite size of 43 nm (Grzmil et al., 2007).

**Table 3**. Crystallite size of zinc phosphate nanoparticles

| Sample Code | Crystallite Size (nm) |
|---|---|
| ZP-DF5 | 38.96 |
| ZP-DF10 | 37.48 |
| ZP-DF20 | 40.32 |
| ZP-DF30 | 42.99 |
| ZP-DF40 | 44.19 |
| ZP-DF50 | 37.98 |

### 2.3. Morphological Analysis of Zinc Phosphate Nanoparticles

SEM analysis of the synthesized zinc phosphate showed the morphology of each test sample. It is apparent from the analysis that some samples have aggregate forms. The ZP-DF10 sample shows a morphology with small grains and is randomly distributed at 1000× magnification of observation (Figure 6).

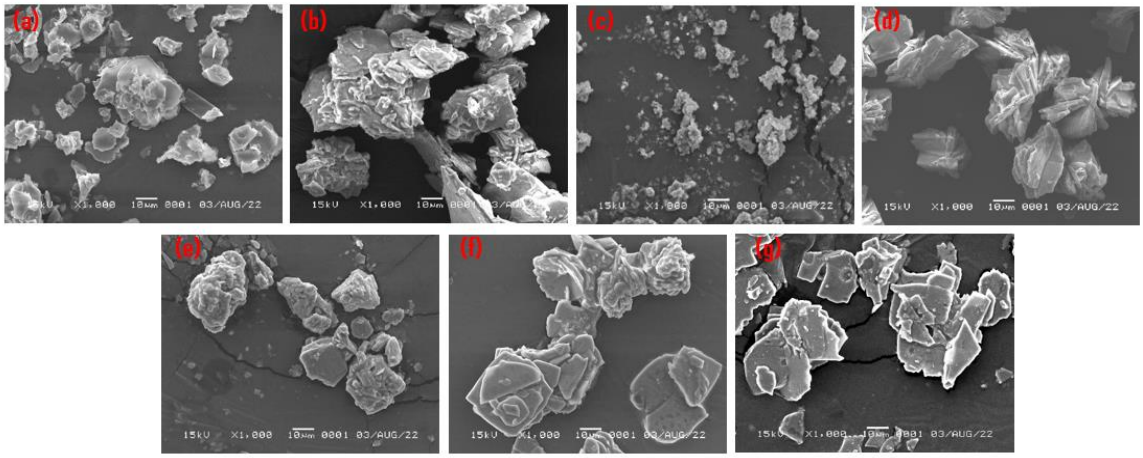


**Figure 6.** The results of the analysis of ZP-dragon fruit peel nanoparticles: (a) ZP, (b) ZP-DF5, (c) ZP-DF10, (d) ZP-DF20, (e) ZP-DF30, (f) ZP-DF40, (g) ZP-DF50.


DOI:https//doi.org/10.22452/mjs.vol43no1.3
Malaysian Journal of Science 43(1): 22-33 (March 2024)

**Synthesis of Bacterial Cellulose-Zinc Phosphate Composite Film**

BC is a layer of cellulose, which is a secondary metabolite formed by *Acetobacter xylinum* microorganisms through the fermentation process. Cellulose is a polysaccharide consisting of (1-4)-glucoside chains. BC can be produced from the activity of bacteria from the Acetobacter, Rhizobium, Agrobacterium, and Sarcina groups (Lippi et al., 2022).

The color of nata produced after soaking is yellowish-white with a slippery surface. Soaking with NaOH aims to create an alkaline atmosphere and raise the pH so that the *Acetobacter xylinum* bacteria are eliminated. Additionally, it aims to get rid of bacteria and non-cellulose elements that could interfere with the cellulose molecular chains' ability to form membrane bonds.

A BC membrane that has been composited forms a color that varies according to the color of the nanoparticle sample used in immersion. It ranges from white to yellow and orange to brown, which visually shows that the BC membrane has been distributed with zinc phosphate nanoparticles.

BC acts as a membrane that will stabilize the size of nanoparticles. In addition, BC has been used as a stabilizing agent that plays a role in the formation of nano-sized particles. The BC-ZP-red dragon fruit peel extract composite film was pressed with a hot press to form a film as shown in Figure 7.

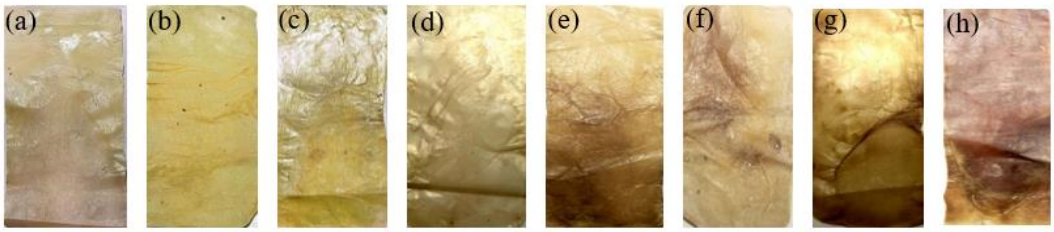


**Figure 7.** BC-zinc phosphate-red dragon fruit peel extract composite films: (a) BC-ZP, (b) BC-ZP-DF5, (c) BC-ZP-DF10, (d) BC-ZP-DF20, (e) BC-ZP-DF30, (f) BC-ZP-DF40, (g) BC-ZP-DF50, (h) BC-Extract.

Furthermore, the success of composite film synthesis is proven by FTIR Spectroscopy (Figure 8). The spectrum of pure BC film was compared with the spectrum of the composite film BC-ZP-DF10; the most significant peak change was seen between the FTIR spectrum of the pure BC film and the composite film BC-ZP-DF10. For pure BC spectrum at wavenumbers of 3345 $cm^{-1}$ to 2902 $cm^{-1}$, it shows the presence of –OH stretching. However, in the FTIR spectrum for BC-ZP-DF10 composite, the OH peak is not as wide as exhibited in the pure BC spectrum because some of the –OH has interacted with zinc phosphate. In the BC spectrum, it is also clear that there are wide peaks at 2800 $cm^{-1}$ to 2900 $cm^{-1}$ indicating C-H stretching, 1160 $cm^{-1}$ indicating C-O-C stretching, and 1035 $cm^{-1}$ to 1060 $cm^{-1}$ indicating C=O stretching. In the BC-ZP-DF10 spectrum, it is clear that there is a sharp peak at a wavenumber of 1391 $cm^{-1}$ which is the characteristic peak of $PO_4^{3-}$. The wide band is exhibited at 500 ~ 700 $cm^{-1}$ indicating the presence of $PO_4^{3-}$ flexural and Zn strain vibration groups. Therefore, the composite film that was synthesized exhibits the successful integration of zinc phosphate nanoparticles into the BC Film.

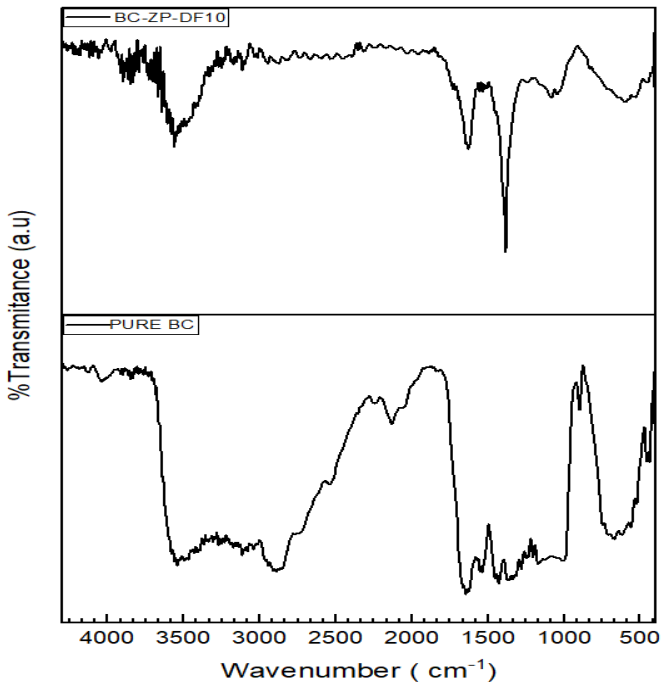


**Figure 8.** FTIR spectrum of composite films: (A) BC-ZP-DF10,


DOI:https//doi.org/10.22452/mjs.vol43no1.3
Malaysian Journal of Science 43(1): 22-33 (March 2024)

(B) Pure BC Film.

Morphological analysis was conducted to determine the morphology of the composite film in the form of pores and particle size on the BC-ZP-DF10, which greatly influences the effectual properties of the membrane that role as a filter and composite as an antibacterial. The pore size of the membrane significantly affects the number of metal nanoparticles deposited in it (Ottenhall et al., 2018). The results of the morphological analysis using a Digital Optic Microscope are shown in Figure 9.

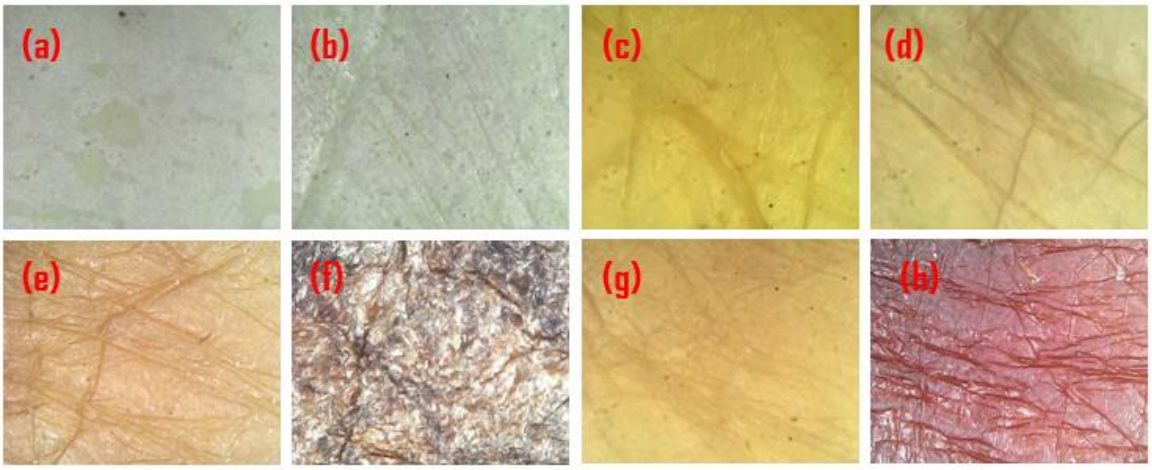


**Figure 9.** Digital microscope analysis results of BC-ZP-red dragon fruit peel extract composite films: (a) BC-ZP, (b) BC-ZP-DF5, (c) BC-ZP-DF10, (d) BC-ZP-DF20, (e) BC-ZP-DF30, (f) BC-ZP-DF40, (g) BC-ZP-DF50, (h) BC-Extract.

This analysis shows an even distribution of zinc phosphate nanoparticles on the surface of BC. A very good distribution pattern is also shown in the film BC-ZP-DF10. The ZP-DF10 nanoparticles, which have the smallest size, were strengthened from the morphological analysis of ZP-DF10 nanoparticles using SEM (Figure 6), allowing them to be easily distributed into the pores of the BC membrane. Therefore, to further prove the formation of the composite film, the BC-ZP-DF10 composite film, and pure BC film were further tested for their morphology using SEM. Figure 10a displays the results of the SEM analysis of pure BC. From the morphology image of BC, it is evident that the pores are still empty. After being composited with nanoparticles, it is clear that the pores are evenly filled with ZP-DF10 nanoparticles (Figure 10b).

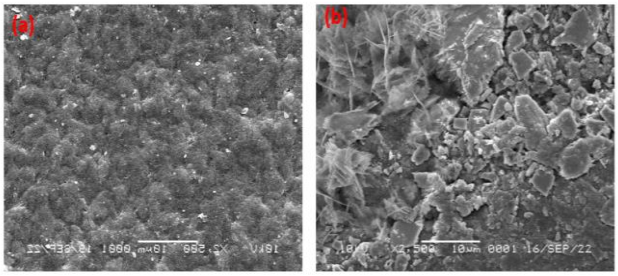


**Figure 10.** The results of the analysis of the morphology of the film: (A) Pure BC Film, (B) Composite film of BC-ZP-DF10.

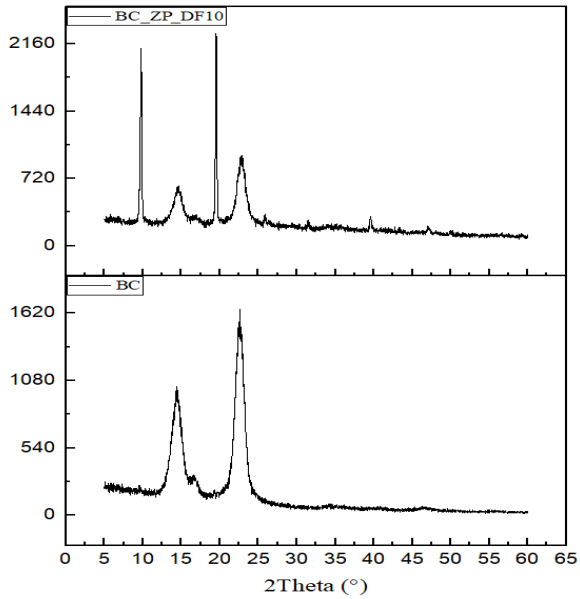


**Figure 11.** XRD spectrum of composite: (a) Composite film of BC-ZP-DF10, (b) Pure BC.

Figure 11 shows that there is a difference between peak two theta on BC and BC-ZP-DF10 composite. The XRD spectrum of the BC filter shows a semicrystalline phase with a little wide peak at two theta of 14.48º and 22.62º. After incorporation with zinc phosphate, the peak change that there is the additional peak of two theta of 9.78º, 19.48º, 39.63º, and 47.17º, while the peak intensity of the semicrystalline phase reduced. This finding clarifies the profile from FTIR data and SEM morphology. It also proves that zinc phosphate is incorporated in the cellulose BC framework as well.


DOI:https//doi.org/10.22452/mjs.vol43no1.3
Malaysian Journal of Science 43(1): 22-33 (March 2024)

**Antimicrobial Activity Test**

The synthesized zinc phosphate and composite samples were tested for their antibacterial activities against *S. aureus* (Figure 12) and *P. aeruginosa* (Figure 13).

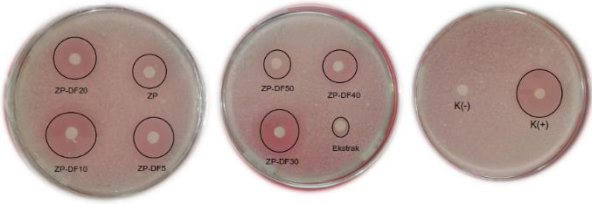


**Figure 12.** *S. aureus* antibacterial test results on samples ZP, ZP-DF5, ZP-DF10, ZP-DF20, ZP-DF30, ZP-DF40, ZP-DF50, and red dragon fruit peel extract.

**Figure 13.** *P. aeruginosa* antibacterial test results on samples ZP, ZP-DF5, ZP-DF10, ZP-DF20, ZP-DF30, ZP-DF40, ZP-DF50, and red dragon fruit peel extract.

The results of antibacterial activity tests of zinc phosphate nanoparticles are displayed in Table 4. Based on the results, all test samples noticeably inhibited the growth of *S. aureus* and *P. aeruginosa*, except for the negative control. The ZP-DF10 test sample had the most potent antibacterial activity of all samples. Based on this finding, further characterization for composite films only used two samples, namely BC and ZP-DF10.

**Table 4**. Average diameter of inhibition zone of zinc phosphate nanoparticle samples-red dragon fruit peel extract

| **Indicator Bacteria** | **Test Sample** | Diameter of Inhibition Zone **(mm)** | **Indication** |
|---|---|---|---|
| *S. aureus* | ZP | 14.02 | Strong |
| | ZP-DF5 | 21.35 | Very strong |
| | ZP-DF10 | 23.69 | Very strong |
| | ZP-DF20 | 19.36 | Strong |
| | ZP-DF30 | 17.00 | Strong |
| | ZP-DF40 | 14.36 | Strong |
| | ZP-DF50 | 10.69 | Strong |
| | Extract | 8.35 | Moderate |
| | (+)Tetracycline | 26.03 | Very strong |
| | (-) Distillate Water | - | - |
| *P. aeruginosa* | ZP | 10.68 | Moderate |
| | ZP-DF5 | 13.37 | Strong |
| | ZP-DF10 | 14.68 | Strong |
| | ZP-DF20 | 11.69 | Strong |
| | ZP-DF30 | 8.02 | Moderate |
| | ZP-DF40 | 8.35 | Moderate |
| | ZP-DF50 | 7.03 | Moderate |
| | Extract | 8.34 | Moderate |
| | (+)Tetracycline | 29.01 | Very strong |
| | **(-)**Distillate Water | - | - |

Based on the diameter of inhibition zone measurements, the results of the antimicrobial activity test of BC-ZP-dragon fruit extract nanocomposite film revealed that all test samples had excellent bacterial growth inhibition against *S. aureus* (Figure 14 and Table 5). ZP-DF10 had the widest inhibition zone among all test samples, which was equal to 21.35 mm. However, after testing the widest inhibitory zone for *P. aeruginosa*, the inhibition zone was classified as weak in each test sample (Figure 15 and Table 5).

**Figure 14.** The results of the antibacterial activity test of film BC-ZP-DF5, BC-ZP-DF10, BC-ZP-DF20, BC-ZP-DF30, BC-ZP-DF40, BC-ZP-DF50, BC-ZP, and red dragon fruit peel extract to *S. aureus* bacteria.


DOI:https//doi.org/10.22452/mjs.vol43no1.3
Malaysian Journal of Science 43(1): 22-33 (March 2024)

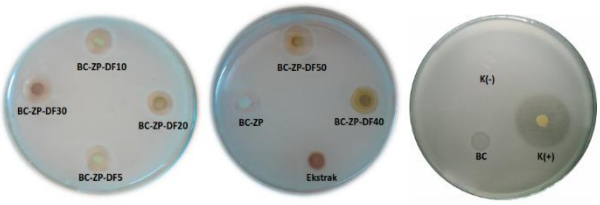


**Figure 15.** The results of the antibacterial activity test of film BC-ZP, BC-ZP-DF5, BC-ZP-DF10, BC-ZP-DF20, BC-ZP-DF30, BC-ZP-DF40, BC-ZP-DF50, and red dragon fruit peel extract to *P. aeruginosa* bacteria.

**Table 5**. Average diameter of inhibition zone of bacteria growth on the zinc phosphate nanoparticle composite film

| **Indicator bacteria** | **Composite** | Diameter of Inhibition Zone **(mm)** | **Indication** |
|---|---|---|---|
| *S. aureus* | BC-ZP | 14.02 | Strong |
| | BC-ZP-DF5 | 17.50 | Strong |
| | BC-ZP-DF10 | 21.35 | Very strong |
| | BC-ZP-DF20 | 19.36 | Strong |
| | BC-ZP-DF30 | 17.00 | Strong |
| | BC-ZP-DF40 | 7.42 | Strong |
| | BC-ZP-DF50 | 11.69 | Strong |
| | Extract | 8.35 | Moderate |
| | (+)Tetracycline | 26.13 | Very strong |
| | (-) Distillate Water | - | - |
| *P. aeruginosa* | BC-ZP | 3.51 | Weak |
| | BC-ZP-DF5 | 4.26 | Weak |
| | BC-ZP-DF10 | 3.84 | Weak |
| | BC-ZP-DF20 | 3.53 | Weak |
| | BC-ZP-DF30 | 2.73 | Weak |
| | BC-ZP-DF40 | 2.83 | Weak |
| | BC-ZP-DF50 | 2.34 | Weak |
| | Extract | 2.83 | Weak |
| | (+)Tetracycline | 29.28 | Very strong |
| | **(-)**Distillate Water | **-** | **-** |

**Air Filter Efficiency Test**

Performance analysis of the air filter of the BC-zinc phosphate composite film aimed to evaluate the separation of particulate materials based on their molecular size and shape. The composite film retains particulate components from the feed that are larger than the membrane pores and passes the smaller ones.

The performance of the air filter media is indicated by the results of the efficiency measurement. This is expressed by Equation (2), where %*E* is the percent of efficiency and *Cf* and *Ci* are the numbers of particles after and before passing through the filter, respectively. The results of the air filter performance test of the BC-zinc phosphate nanoparticles composite are presented in Figure 16.

Performance testing of the film filter samples for cellulose of nata de coco, BC-ZP, NC-Extract, BC-ZP-DF5, BC-ZP-DF10, BC-ZP-DF20, BC-ZP-DF30, BC-ZP-DF40, and BC-ZP-DF50 showed that the average efficiency of the composite film were 79.80%, 84.33%, 86.73%, 83.44%, 90.10%, 85.87%, 88.87%, 86.56%, and 88.26%, respectively (Figure 16). The incorporation of zinc phosphate on the cellulose filter increased the filtering efficiency until BC-ZP-DF10 and then decreased on BC-ZP-DF20. This is presumably because the crystal size of the zinc phosphate nanoparticles started to increase and aggregate on the surface of the BC cellulose filter (shown in Table 3 and Figure 6), resulting in a less even distribution on the composite film surface. The capability of the film as an antibacterial material was an additional advantage in particulate matter filter application.

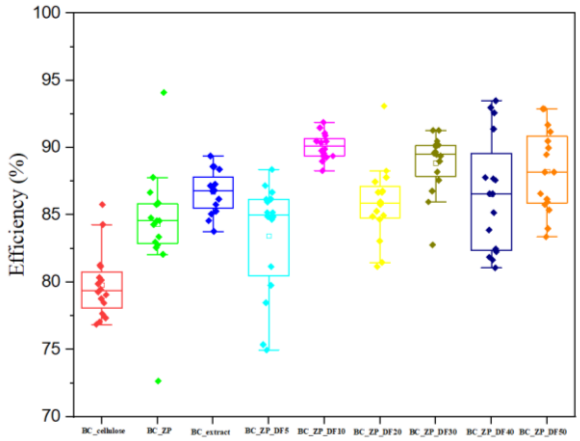


**Figure 16.** Air filter test of the composite film

## 4. Conclusion

In this study, the synthesis of zinc nanoparticles through a green chemistry approach was carried out by reacting a red dragon fruit peel extract with a zinc phosphate solution. The results of UV-Vis analysis showed that the absorbance values for 30 minutes tended to be stable. Functional group analysis using FTIR demonstrated the presence of functional group interactions between the compounds in the red dragon fruit peel extract and zinc phosphate. The results of XRD analysis showed that the peak of two thetas at 9.54º, 19,93º, and 31,26º indicate the typical presence of zinc phosphate. The estimated crystallite size analyzed from XRD shows that ZP-DF10 has an average-sized crystal with the smallest value of 37.48 nm. The red dragon fruit peel extract nanoparticles composited with BC film showed morphological differences with the pure BC film. The SEM test revealed that BC had empty pores. After being composited with nanoparticles, it was clear that the pores were evenly filled with ZP-DF10 nanoparticles. The XRD spectrum of the BC film showed a semicrystalline phase with a little wide peak at two theta of 14.48º and 22.62º. After incorporation with zinc phosphate, the peak change that there is the additional peak of two theta of


DOI:https//doi.org/10.22452/mjs.vol43no1.3
Malaysian Journal of Science 43(1): 22-33 (March 2024)

9.78º, 19.48º, 39.63º, and 47.17º, while the peak intensity of the semicrystalline phase reduced. This finding clarifies the profile from FTIR data and SEM morphology, and it also proves that zinc phosphate is incorporated in the cellulose BC framework. Antimicrobial activity tests of nanocomposite films using *S. aureus* and *P. aeruginosa* bacteria confirmed that all compositions had good inhibitory properties, and composite film NC-ZP-DF10 had the strongest inhibition. The results of the air filter test for particulate matter demonstrated that the best average efficiency of the BC-zinc phosphate nanoparticles composite is 90.10%.

## 5. Acknowledgements

The author would like to thank the Ministry of Education, Culture, Research and Technology of the Republic of Indonesia, especially the Directorate of Research and Community Service for the research grant in accordance with the Research Program Implementation Contract Number: 108/E5/PG. 02.00.PT/2022 dated 10 May 2022. We would also like to thank the Institute for Research and Community Service at Halu Oleo University.

## 6. References

Budi, P. (2017). Biosynthesis of Silver Nanoparticles Using Ketapang Leaf Extract, Modification With P- Coumaric Acid For Detecting Melamine. *Indonesian Journal of Chemical Science*, *4*(2), 367–372.

Dil, M. A., Haghighatzadeh, A., & Mazinani, B. (2019). Photocatalytic Activity of Aeroxide TiO2 Sensitized By Natural Dye Extracted From Mangosteen Peel. *Bulletin of Materials Science*, *42*(5). https://doi.org/10.1007/s12034-019-1927-9

Franchitti, E., Pascale, E., Fea, E., Anedda, E., & Traversi, D. (2020). Methods For Bioaerosol Characterization: Limits And Perspectives For Human Health Risk Assessment In Organicwaste Treatment. *Atmosphere*, *11*(5). https://doi.org/10.3390/ATMOS11050452

Ghosh, M., Chowdhury, P., & Ray, A. K. (2020). Photocatalytic Activity of Aeroxide TiO2 Sensitized By Natural Dye Extracted From Mangosteen Peel. *Catalysts*, *10*(8). https://doi.org/10.3390/catal10080917

Grzmil, B., Kic, B., & Lubkowski, K. (2007). Studies on Obtaining of Zinc Phosphate Nanomaterials. *Reviews on Advanced Materials Science*, *14*(1), 46–48.

Haiss, W., Thanh, N. T. ., Jenny, A., & Fernig, D. G. (2008). Determination of Size and Concentration of Gold Nanoparticles from UV-Vis Spectra. *Zidonghua Xuebao/ Acta Automatica Sinica*, *34*(9), 1040–1046. https://doi.org/10.3724/SP.J.1004.2008.01040

Horky, P., Skalickova, S., Urbankova, L., Baholet, D., Kociova, S., Bytesnikova, Z., Kabourkova, E., Lackova, Z., Cernei, N., Gagic, M., Milosavljevic, V., Smolikova, V., Vaclavkova, E., Nevrkla, P., Knot, P., Krystofova, O., Hynek, D., Kopel, P., Skladanka, J., … Smerkova, K. (2019). Zinc phosphate-based nanoparticles as a novel antibacterial agent: In vivo study on rats after dietary exposure. *Journal of Animal Science and Biotechnology*, *10*(1), 1–12. https://doi.org/10.1186/s40104-019-0319-8

Jonsirivilai, B., Torgbo, S., & Sukyai, P. (2022). Multifunctional filter membrane for face mask using bacterial cellulose for highly efficient particulate matter removal. *Cellulose*, *29*(11), 6205–6218. https://doi.org/10.1007/s10570-022-04641-3

Kimbonguila, A., Matos, L., Petit, J., Scher, J., & Nzikou, J.-M. (2019). Effect of Physical Treatment on the Physicochemical, Rheological and Functional Properties of Yam Meal of the Cultivar "Ngumvu" From Dioscorea Alata L. of Congo. *International Journal of Recent Scientific Research*, *10*(October), 30693–30695. https://doi.org/10.24327/IJRSR

Konda, A., Prakash, A., Moss, G. A., Schmoldt, M., Grant, G. D., & Guha, S. (2020). Aerosol Filtration Efficiency of Common Fabrics Used in Respiratory Cloth Masks. *ACS Nano*, *14*(5), 6339–6347. https://doi.org/10.1021/acsnano.0c03252

Kopel, P., Cernei, N., Gagic, M., Horky, P., Smerkova, K., & Adam, V. (2018). Zinc phosphate nanoparticles preparation and their antimicrobial activity. *Nanocorn 2018 Conference Proceedings*.

Lippi, M., Riva, L., Caruso, M., & Punta, C. (2022). Cellulose for the Production of Air-Filtering Systems: A Critical Review. *Materials*, *15*(3). https://doi.org/10.3390/ma15030976

Liu, X., Souzandeh, H., Zheng, Y., Xie, Y., Zhong, W. H., & Wang, C. (2017). Soy protein isolate/bacterial cellulose composite membranes for high efficiency particulate air filtration. *Composites Science and Technology*, *138*, 124–133. https://doi.org/10.1016/j.compscitech.2016.11.022

Manihuruk, F. M., Suryati, T., & Arief, I. I. (2017). Effectiveness of the red dragon fruit (Hylocereus polyrhizus) peel extract as the colorant, antioxidant, and antimicrobial on beef sausage. *Media Peternakan*, *40*(1), 47–54. https://doi.org/10.5398/medpet.2017.40.1.47

Manoukian, O. S., Sardashti, N., Stedman, T., Gailiunas, K., Ojha, A., Penalosa, A., Mancuso, C., Hobert, M., & Kumbar, S. G. (2019). Biomaterials for tissue engineering and regenerative medicine. In *Encyclopedia of Biomedical Engineering* (Vols. 1–3). Elsevier Inc. https://doi.org/10.1016/B978-0-12-801238-3.64098-9


DOI:https//doi.org/10.22452/mjs.vol43no1.3
Malaysian Journal of Science 43(1): 22-33 (March 2024)

Massoud, R., & Saffari, H. (2020). Screening methods for assessment of antibacterial activity in nature. *4th International Conference on Applied Researches in Science and Engineering*, *December*, 0–11.

Mulyasuryani, A., & Mustaghfiroh, A. M. (2019). Development of Potentiometric Phenol Sensors by Nata de Coco Membrane on Screen-Printed Carbon Electrode. *Journal of Analytical Methods in Chemistry*, *2019*. https://doi.org/10.1155/2019/4608135

Nugroho, D. A., & Aji, P. (2015). Characterization of Nata de Coco Produced by Fermentation of Immobilized Acetobacter xylinum. *Agriculture and Agricultural Science Procedia*, *3*, 278–282. https://doi.org/10.1016/j.aaspro.2015.01.053

Nurtiana, W. (2019). Anthocyanin As Natural Colorant: a Review. *Food ScienTech Journal*, *1*(1), 1. https://doi.org/10.33512/fsj.v1i1.6180

Onoda, H., & Haruki, M. (2016). Influence of phosphate source on preparation of zinc phosphate white pigments. *International Journal of Industrial Chemistry*, *7*(3), 309–314. https://doi.org/10.1007/s40090-015-0067-3

Ottenhall, A., Henschen, J., Illergård, J., & Ek, M. (2018). Cellulose-based water purification using paper filters modified with polyelectrolyte multilayers to remove bacteria from water through electrostatic interactions. *Environmental Science: Water Research and Technology*, *4*(12), 2070–2079. https://doi.org/10.1039/c8ew00514a

Rahmayanti, H. D., Amalia, N., Munir, R., Yuliza, E., Utami, F. D., Sustini, E., & Abdullah, M. (2019). A Study of Physical and Mechanical Properties of Nata de Coco in the Market. *IOP Conference Series: Materials Science and Engineering*, *599*(1). https://doi.org/10.1088/1757-899X/599/1/012031

Sabherwal, S., Chaku, D., Mathur, U., V, S., & A, M. (2017). Are high-efficiency particulate air (HEPA) filters and laminar air flow necessary in operating rooms to control acute post-operative endophthalmitis? *[1] 'Symposium Recent Advances and Challenges in the Management of Retinoblastoma Globe - Saving Treatments', BMC Ophthalmol., Vol. 17, No. 1, p. 1, 2017, Doi: 10.4103/Ijo.IJO.BMC Ophthalmology*, *17*(1), 1. https://doi.org/10.4103/ijo.IJO

Wang, J. D., Li, D., Liu, J. K., Yang, X. H., He, J. L., & Lu, Y. (2011). One-Step Preparation and Characterization of Zinc Phosphate Nanocrystals with Modified Surface. *Soft Nanoscience Letters*, *01*(03), 81–85. https://doi.org/10.4236/snl.2011.13015

Wu, A., Hu, X., Ao, H., & Chen, Z. (2022). Rational design of bacterial cellulose-based air filter with antibacterial activity for highly efficient particulate matters removal. *Nano Select*, *3*(1), 201–211. https://doi.org/10.1002/nano.202100086

Xing, Y. F., Xu, Y. H., Shi, M. H., & Lian, Y. X. (2016). The impact of PM2.5 on the human respiratory system. *Journal of Thoracic Disease*, *8*(1), E69–E74. https://doi.org/10.3978/j.issn.2072-1439.2016.01.19

Zakir, M., & Budi, P. (2016). Effect of AgNO3 concentration and synthesis temperature on surface plasmon resonance (SPR) of silver nanoparticles. *J. Chem. Res*, *4*(1), 356–361.

Zhang, J., Wang, J., Xu, H., Lv, X., Zeng, Y. X., Duan, J., & Hou, B. (2019). The effective photocatalysis and antibacterial properties of AgBr/AgVO3 composites under visible-light. *RSC Advances*, *9*(63), 37109–37118. https://doi.org/10.1039/c9ra06810d



DOI:https//doi.org/10.22452/mjs.vol43no1.3
Malaysian Journal of Science 43(1): 22-33 (March 2024)